Ceramics International 42 (2016) 8431–8437

Contents lists available at ScienceDirect

Ceramics International

journal homepage: www.elsevier.com/locate/ceramint

Preparation of refractory cordierite using amorphous rice husk silica for thermal insulation purposes

Simon Sembiring [a,*], Wasinton Simanjuntak [b], Rudy Situmeang [b], Agus Riyanto [a], Kerista Sebayang [c]

[a] Department of Physics, Faculty of Mathematics and Natural Sciences, University of Lampung, Jl. Prof. Soemantri Brojonegoro No. 1, Bandar Lampung 35145, Indonesia
[b] Department of Chemistry, Faculty of Mathematics and Natural Sciences, University of Lampung, Prof. Soemantri Brojonegoro No. 1, Bandar Lampung 35145, Indonesia
[c] Department of Physics, Faculty of Mathematics and Natural Sciences, University of North Sumatera, Jl. Bioteknologi No. 1, Kampus Padang Bulan, Medan 20155, Indonesia

ARTICLE INFO

Article history:
Received 27 October 2015
Received in revised form
2 February 2016
Accepted 10 February 2016
Available online 18 February 2016

Keywords:
A. Sintering
D. Cordierite
Rice husk
Structure
Refractory

ABSTRACT

This study aims to investigate the effect of sintering temperatures on the phase formation and physical characteristics of refractory cordierite prepared from rice husk silica, Al_2O_3, and MgO powders. The samples were subjected to sintering temperatures of 1050–1350 °C, and development of structures was characterized using Fourier Transform Infrared (FTIR) spectroscopy, X-ray diffraction (XRD) coupled with Rietveld analysis, scanning electron microscopy (SEM) and dilatometry. The results obtained indicated the significant role of sintering temperatures on phase transformation of spinel and cristobalite into cordierite, in which at sintering temperatures of 1230–1350 °C the cordierite emerges as a dominant phase, while spinel and cristobalite are practically undetected. Formation of cordierite was followed by decrease in density, porosity, and thermal expansion coefficient, while for hardness and bending strength the opposite was true. Thermal expansion coefficient of the sintered sample at 1350 °C is 3.3×10^{-6}/°C and the XRD analysis demonstrated that the main crystalline phase is cordierite. Based on these characteristics, the samples are considered as insulator, suggesting their potential use in refractory devices.

1. Introduction

Cordierite ($Mg_2Al_4Si_5O_{18}$) ceramic is well known as an excellent insulator and high-thermal resistant material, due to its low dielectric constant as well as thermal expansion coefficient. In previous study [1,2], it was reported that thermal expansion of cordierite is 2.2×10^{-6}/°C, while the others reported the value of around $1–4 \times 10^{-6}$/°C [3] and $0.8–2 \times 10^{-6}$/°C [4,5]. Another interesting property of cordierite which makes this material a great importance as refractory material is its very high melting temperature (1460 °C), which is the highest among silicate glass–ceramics [6]. In addition, cordierite exhibits excellent thermal shock resistance [7,8] and high chemical stability [3]. Cordierite can be found in three polymorphic forms, depends on temperature, *i.e.* α-cordierite at high temperature, while β-cordierite and μ-cordierite at low temperature [9,10]. This polymorphism characteristic means that sintering of the substrate at high temperature will lead to conversion of μ-cordierite and β-cordierite into α-cordierite, as the most stable phase. With such properties, cordierite ceramic is considered as a very promising structural materials, suitable for various applications such as catalyst carriers for exhaust gas purification, heat exchanger for gas turbine engines [7,11], refractory for furnaces, electrical and thermal insulation, filter, membranes and heating elements [12,13].

Recognizing the important roles of cordierite in various industrial areas, production of cordierite has been continuously explored, and in general, it is found that the formation of cordierite phase is strongly dependent on the chemical composition, the types of raw material, the presence of impurities, and the preparation methods applied. Many attempts have been devoted to prepare this material from different raw materials using different methods. In previous study [14], solid-state reaction was applied to synthesize cordierite from Al_2O_3, MgO, and SiO_2. In another study [15], cordierite was synthesized from serpertine, kaolinite, and alumina as raw materials, and found that the formation of cordierite was achieved at sintering temperature of 1350 °C. The same formation temperature was reported by others [16] using the

* Corresponding author.
E-mail address: simonsembiring2@gmail.com (S. Sembiring).

http://dx.doi.org/10.1016/j.ceramint.2016.02.062
0272-8842/

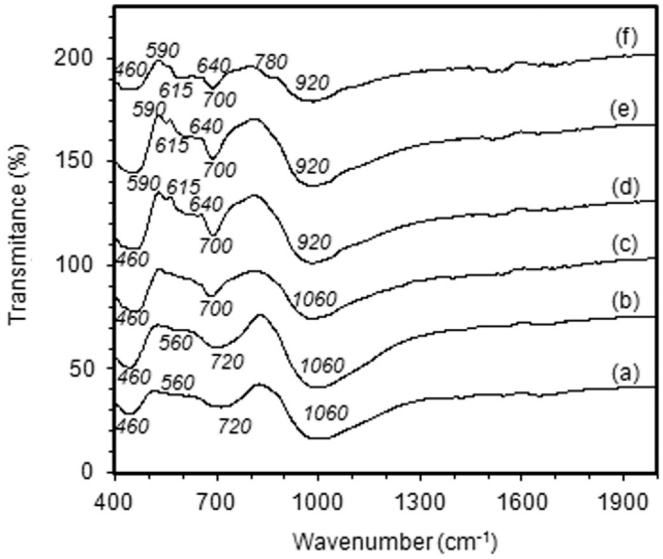

Fig. 1. FTIR spectra of sintered samples at different temperatures (a) 1050 °C, (b) 1110 °C, (c) 1170 °C, (d) 1230 °C, (e) 1290 °C and (f) 1350 °C.

same method but different raw materials, including andalusite and stevensite. Previous study also showed that α-cordierite, $MgAl_2O_4$/spinel and cristobalite formed at 1300 and at 1350 °C, while at 1375 °C the only phase observed was α-cordierite [9]. Several other studies have reported the synthesis of cordierite from a variety of raw materials such as alumina, kaolinite and talcum [17], fumed silica, bauxite, and talcum [18], talcum, kaolinite, fieldspar, and sepiolite [1, 19], and stevensite-rich clay and andalusite using oil shale as a natural pore-forming agent [20].

Beside solid-state reaction, another method that has been extensively applied is sol–gel method. In previous study [21], this method has been applied to prepare cordierite using silicon alkoxide, chelated aluminum sec-butoxide, and magnesium acetate as starting precursors, and found that the initiation of the μ→α cordierite transformation took place in the temperature range of 1000–1100 °C and α-cordierite was produced at 1200 °C. The study using a mixture of aluminum isopropoxide, magnesium ethoxide, and tetraethylorthosilicate in absolute ethanol revealed that μ-cordierite crystallized at temperature range of 950–1000 °C accompanied by the formation of spinel in small amount, and transformation of μ into α-cordierite started at about 1100 °C [22]. In another study [23] synthesis of cordierite from aluminum chloride, magnesium chloride, and tetraethylorthosilicate was reported. The results obtained indicate that crystallization of μ-cordierite occurred at temperatures between 900 and 1000 °C, and transformed into α-cordierite at temperatures in the range of 1400–1450 °C. Slightly different result was reported by others [24], who used silicic acid, magnesium and aluminum salts, as raw materials, in which it was found that μ-cordierite crystallization occurred at 900 °C, followed by the formation α-cordierite at temperature of 1200 °C and complete transformation of μ into α-cordierite at 1350 °C.

In general, the characteristics of refractory cordierite for thermal insulator are influenced by complex relationship between microstructure and crystalline phases having different thermal expansions when subjected to high temperature and under thermal shock condition. In overall, refractory material should exhibit high thermal shock resistance, high fracture toughness, and low thermal expansion. For these reasons, thermal resistance parameters and thermal shock behaviors of refractory cordierite have been the subject of extensive studies. Previous researchers [7,25] have attempted to synthesize cordierite with excellent thermal

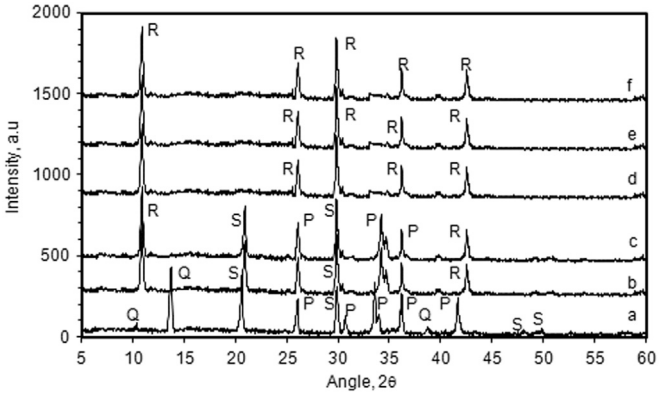

Fig. 2. The x-ray diffraction patterns of the sintered samples at different temperatures (a) 1050 °C, (b) 1110 °C, (c) 1170 °C, (d) 1230 °C, (e) 1290 °C and (f) 1350 °C. P: spinel, Q: μ-cordierite, R: α-cordierite, S: cristobalite.

shock resistance by subjecting the raw materials into rapid and severe changes in temperature. They found that microstructure and sintering temperature strongly influenced the fracture toughness and densification of cordierite. Considerable effort has also been devoted to study the use of cordierite as the component of refractory material for high thermal applications [5,26], and found that the fracture toughness increases with increasing sintering temperature from 1250 to 1300 °C. Suzuki et al. 1992 [27] have successfully prepared cordierite with high purity and homogeneity, after the sample was sintered at 1300 °C

Related to raw materials for preparation of ceramics, rice husk is a very attractive source of silica, primarily since this agriculture residue is abundantly available, renewable, high silica content, and simple extraction of the silica from the husk. In our previous investigations, active silica from rice husk was obtained by simple acid leaching, and the silica has been used to produce several ceramic materials include borosilicate [28], cordierite [29], carbosil [30], aluminosilicate [31], and mullite [32,33]. The potential of rice husk as an excellent source of high-grade amorphous silica has also been investigated in many other studies [34–36]. Furthermore, this silica has been utilized for preparation of various valuable materials such as solar grade silicon [37], silica carbide [38], magnesium–alumina–silica [39], and lithium–aluminum–silica [40].

To take advantage of the its availability and excellent properties, this present study is aimed to evaluate the potential of rice husk silica as an alternative to commonly used silica for production of cordierite as refractory material for thermal insulation purposes using solid-state reaction. The precursors produced then subjected to thermal treatment in order to investigate the phase development and physical properties. To gain insight on several basic characteristics, the samples were characterized using various techniques include FTIR spectroscopy for functionality analysis, XRD technique for structure investigation, and SEM technique for microstructure investigation.

2. Experimental methods

2.1. Materials

Raw husk used as a source of silica was from local rice milling industry in Bandar Lampung Province, Indonesia. Al_2O_3, MgO powders, KOH, HCl, and absolute alcohol (C_2H_5OH) were purchased from Merck (kGaA, Damstadt, Germany).

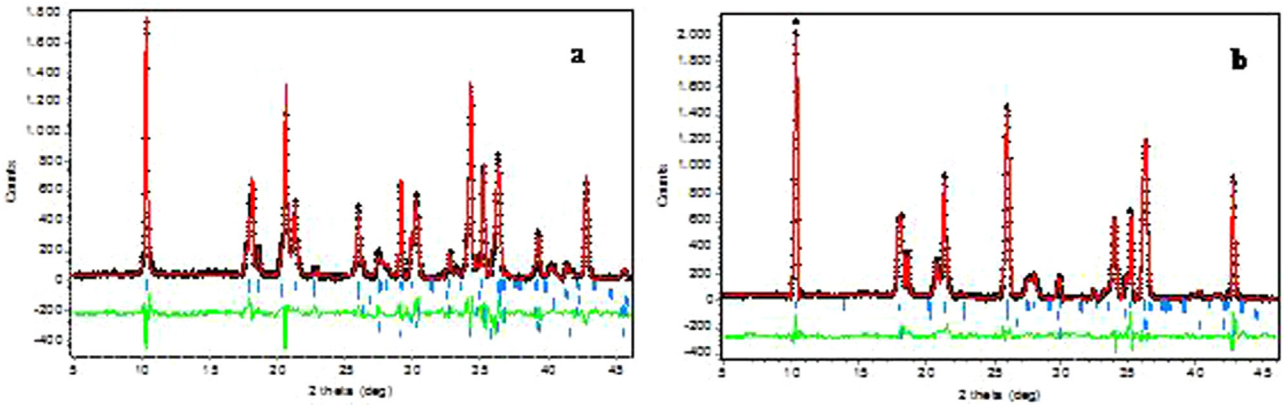

Fig. 3. XRD Rietveld plot for the sample sintering at temperature (a) 1110 °C and (b) 1350 °C. The observed data are shown by the (+) sign, and the calculated data by a solid line.

2.2. Procedure

2.2.1. Preparation of silica powder from rice husk

Rice husk silica was obtained using alkali extraction method following the procedure reported in previous study [28,33]. For extraction, 50 g dried and cleaned husk was mixed with 500 ml of 5% KOH solution in a beaker glass, followed by boiling of the mixture for 30 min. To optimize the extraction of the silica, the mixture was allowed to cool to room temperature and left for 24 h, followed by filtration using Millipore filter to separate the silica sol from the residual husk. The sol was acidified by dropwise addition of 5% HCl solution until conversion of the sol into gel was completed. The obtained gel was left for three days for aging, and then rinsed repeatedly with deionised water to remove the excess of acid. The gel was oven dried at 110 °C for eight hours and then ground into powder.

2.2.2. Preparation of cordierite

Preparation of cordierite was carried out by mixing raw materials with the composition of $MgO:Al_2O_3:SiO_2$ of 2:2:5 by mass, in accordance with the composition of cordierite as reported in previous studies [12,29]. The raw materials were mixed with alcohol under magnetic stirring for 6 h. After the completion of the mixing process, the mixture was filtered and the solid was oven dried at 110 °C for eight hours to remove the adsorbed alcohol. The solid was ground into powder by mortar and sieved to obtain the powder with the size of 200 meshes. The powder was pressed in a metal die with the pressure of 2×10^4 N/m^2 to produce cylindrical pellet and the pellets were sintered at temperatures of 1050, 1110, 1170, 1230, 1290, and 1350 °C, using temperature programmed with a heating rate of 3 °C/min and holding time of 4 h at peak temperatures.

2.3. Characterization

A Perkin Elmer FTIR was used to investigation of functional groups. The sample was prepared by mixing with KBr of spectroscopy grade, and scanning the spectral range of 4000–400 cm^{-1}. The structure analysis was carried out using an automated Shimadzu XD-610 X-ray diffractometer at the National Agency for Nuclear Energy (BATAN), Serpong-Indonesia. The operating conditions used were CuKα radiation ($\lambda = 0.15418$), produced at 40 kV and 30 mA, with a 0.15° receiving slit. Patterns were recorded over goniometric (2θ) ranges from 5° to 80° with a step size of 0.02, counting time 1 s/step, and using post-diffraction graphite monochromator with a NaI detector. The diffraction data were analyzed using JADE software after subtracting the background and stripping the CuKα2 pattern [41] and the refinements were performed using the Rietica program for Windows 95/98/NT version1.70 [42]. The crystal structure models used in the calculation were taken from the Inorganic Crystal Structure Data Base [43].

Microstructural analysis was conducted with SEM Philips-XL, on polished and thermally etched samples. The examination of porosity and density was done according to Archimedes method [44]. A Zwick tester was used to measure the Vickers hardness, with three replicate measurements for each loading position. Bending strength or Modulus Rupture (MOR) was determined by the triple point method following the ASTM C268-70. The measuring of thermal expansion coefficient was conducted using dilatometry (Harrop Dilatometer), in the temperature range of 150–600 °C at a heating rate of 5 °C/min. The linear thermal expansion coefficient (α) was automatically calculated using the general equation: $\alpha = (\Delta L/L)(1/\Delta T)$ where: (ΔL) is the increase in length, (ΔT) is the temperature interval over which the sample is heated and (L) is the original length of the specimen.

3. Results and discussions

3.1. Characteristics of synthesized refractory cordierite

To study phase development, the samples subjected to sintering treatment at different temperatures were characterized using FTIR, XRD and SEM. The FTIR spectra in the wave number region of 2000–400 cm^{-1} are shown in Fig. 1(a)–(f). Fig. 1(a) shows a broad absorption band located at range of 1100–1000 cm^{-1}, which corresponds to the stretching vibration of Si–O–Si and supported by the appearance of absorption at 460 cm^{-1}, as also mentioned in the literature [45]. In addition, the wide and weak peak located at 700 cm^{-1} is commonly assigned to the stretching Al–O or Mg–O indicating the presence of Mg–O–Al–O-Si bond. The other authors reported that the bands centered at 720 cm^{-1} is associated with the formation SiO_4 tetrahedral and Mg–O–Al–O–Si bond [46]. Fig. 1(b)–(f) indicates the significant effect of thermal treatments on the functionality of the samples. The most obvious change is the shift of peaks associated with Al–O and Mg–O bonds, accompanied by the emergence of new peaks at 640, 615, 590, 460, and 430 cm^{-1}, assigned to Mg–O–Al–O–Si stretching modes (Fig. 1(d)–(f)). These bands increase with increasing sintering temperatures, confirming the existence of $MgO \cdot Al_2O_3 \cdot SiO_2$ structure, as suggested in previous studies [22,47].

Fig. 2(a)–(f) displays the XRD patterns of the samples sintered at different temperatures. The phases identified with the PDF diffraction lines using search-match method [48], clearly show the presence of spinel (PDF-21-11520) with the most intense peak at $2\theta = 36.92°$, μ-cordierite (PDF-14-0249) at $2\theta = 13.45°$, α-cordierite

Table 1
Figure-of merits (FOMS) from refinement of XRD Data for the samples sintered at different temperatures for 6 h.

Temp (°C)	R_{exp}	R_{wp}	Rp	GoF
1050	11.36	14.34	11.76	1.58
1110	9.19	11.52	11.41	1.56
1170	8.42	10.85	10.79	1.63
1230	9.52	10.25	11.56	1.21
1290	9.36	10.92	10.75	1.34
1350	9.46	9.87	9.65	1.08

Table 2
Weight percentage (wt%) from refinement of XRD data for the samples sintered at different temperatures for 6 h. Estimated errors for the least significant digits are given in parentheses. [P: spinel, Q: μ-cordierite, R: α-cordierite, S: cristobalite].

Temp (°C)	R	S	P	Q
1050	–	39.7[1]	32.9[5]	28.4[8]
1110	30.8[1]	40.1[5]	29.1[1]	–
1170	33.8[1]	39.6[4]	26.6[5]	–
1230	90.5[3]	4.7[4]	4.8[2]	–
1290	91.8[2]	3.9[6]	4.3[4]	–
1350	92.7[4]	3.8[2]	4.2[3]	–

(PDF-13-0294) at $2\theta = 10.48°$, and cristobalite (PDF-39-1425) at $2\theta = 21.2°$. At 1050 °C (Fig. 2a) several phases with a noticeable amount of μ-cordierite, spinel and cristobalite are clearly detected while α-cordierite is practically undetected. However, the presence of μ-cordierite is an indication that the reaction has started toward the development of the α-cordierite phase. The presence of cristobalite is most likely as a result of rice husk silica crystallization during the heating, while the presence of μ-cordierite may be the consequence of inter-diffusion between spinel and cristobalite, and the spinel was formed by interaction of AlO_6 and MgO_6 octahedral [22,47,49]. At 1110 °C, the μ-cordierite was changed into α-cordierite, and followed by the formation spinel and cristobalite phases. These phases remained the same to 1170 °C. A further decrease in the μ-cordierite phase following the increases in sintering temperatures reflects the more intensive augmentation of α-cordierite phase formation as well as spinel and cristobalite. This behavior was attributed to the phase transformation of μ-cordierite phase, leading to formation of Mg–O–Al–O–Si bond of α-cordierite phase in the sample. Further increase of sintering temperature from 1230 to 1350 °C caused the spinel and cristobalite phases disappeared almost completely, leading to formation of α-cordierite. This finding is in agreement with the result of previous study [50], in which it was suggested that the formation of α-cordierite is most likely as a result of inter-diffusion between cristobalite and spinel.

In order to obtain quantitative composition, Rietveld refinement of XRD data was performed by the Rietica program version1.70 [42]. After observation and calculation, the refined XRD patterns of the samples sintered at 1110 and 1350 °C are shown in Fig. 3(a)–(b). The best figures-of-merit for all samples were compiled in Table 1. As indicated in Table 1, the results of refinement converged for all samples with satisfactory values of goodness of fit (GOF) as required by Rietveld analysis. The goodness-of fit (GoF) (Table 1) values were relatively low, *i.e* all approximately less than 2%, which is considered as acceptable according to basic principle of GoF less than 4% and R_{wp} less than 20% [51,52]. These results also provide quantitative information regarding the phases present in the sample, therefore could distinguish the phase composition of the samples sintered at different temperatures. Table 2 summarizes the weight percentage (wt%) of various phases formed in all samples at different sintering temperatures. As shown in Table 2, the amount of cordierite increased as the sintering temperature increased from 1110 to 1350 °C, suggesting that the phase crystallized at 1110 °C to produce more cordierite. It was also noticed that higher sintering temperature led to reduced amount of cristobalite and spinel, while the amount of cordierite increased. This result implies that more cristobalite reacted with spinel to form cordierite. The reaction between cristobalite and spinel was clearly indicated by the presence of only small amount of cristobalite and spinel in the sample heat-treated from 1230 to 1350 °C.

The surface morphologies of the sintered samples at different temperatures were characterized using SEM. The micrographs presented in Fig. 4(a)–(f) demonstrates significant effect of sintering temperatures on the size and distribution of the particles on the surface. As displayed by the images in Fig. 4(a)–(c), the surfaces morphologies of the samples are marked by the existence of particles with different grain sizes and distributions. The microstructure of the sample sintered at 1050 °C (Fig. 4a) reveals quite different characteristic to that of the sample treated at 1110 °C (Fig. 4b). The sample prepared at 1050 °C (Fig. 4a) is marked by small grains with less evident grain boundaries, compared to those observed for the other two samples (Fig. 4b–c). In addition, it is obvious that the clusters in the sample prepared at 1050 °C are surrounded by middle and fine grains. The large clusters are most likely composed of μ-cordierite, while the middle and fine grains are spinel and cristobalite, respectively. The surface of samples prepared at higher temperatures (1110 and 1170 °C) are dominated by larger grains composed of α-cordierite clusters and covered some fine grains of cristobalite and spinel. Both samples are marked by initiated coalescence of α-cordierite as a result of μ-cordierite crystallization. This feature suggests that at 1110 and 1170 °C, the cristobalite and spinel phases continue to change and allowed the particles to rearrange, leading to initiation of the formation of α-cordierite. This change is supported by the result of XRD analysis for the sample sintered at 1050 °C presented in Fig. 2a, in which no α-cordierite was detected. The formation α-cordierite can be seen more clearly by inspecting the SEM micrographs of the samples treated at temperature range of 1230–1350 °C (Fig. 4d–f), which display intensified agglomeration on the entire surface as the temperatures increased. This agglomeration led to intensified formation of α-cordierite as indicated by the XRD results (Table 2). This agglomeration phenomenon demonstrated that at the temperature range of 1230–1350 °C, the cristobalite phase has started to melt and reacted with the spinel phase to form α-cordierite. Moreover, the microstructure of the samples was found to display grains with relatively uniform sizes with glassy surface without evident grain boundaries. These surface characteristics suggested that at these temperatures the cristobalite phase has been converted into liquefied silica which penetrated the spinel phase, thus promoting the formation of α-cordierite as the dominant phase, as verified by the XRD results (See Table 2). With the Rietveld calculation, it was found that the quantity of cordierite increased sharply from 30.8 to 92.7 wt% as temperature increased from 1110 to 1350 °C.

3.2. Physical characteristics of synthesized refractory cordierite

The physical properties of the sintered samples at different temperatures are shown in Figs. 5(a)–(b), 6(a)–(b) and 7. Fig. 5(a)–(b) shows the changes in density and porosity of the samples as a function of sintering temperatures. As can be observed, the density and porosity of the sintered samples decrease sharply as the sintering temperatures increase up to 1230 °C, and beyond this temperature, relatively plat lines of the two characteristics were observed up to 1350 °C sintering temperature. As shown in Fig. 5a, the densities of the sintered samples decrease from 3.50 to

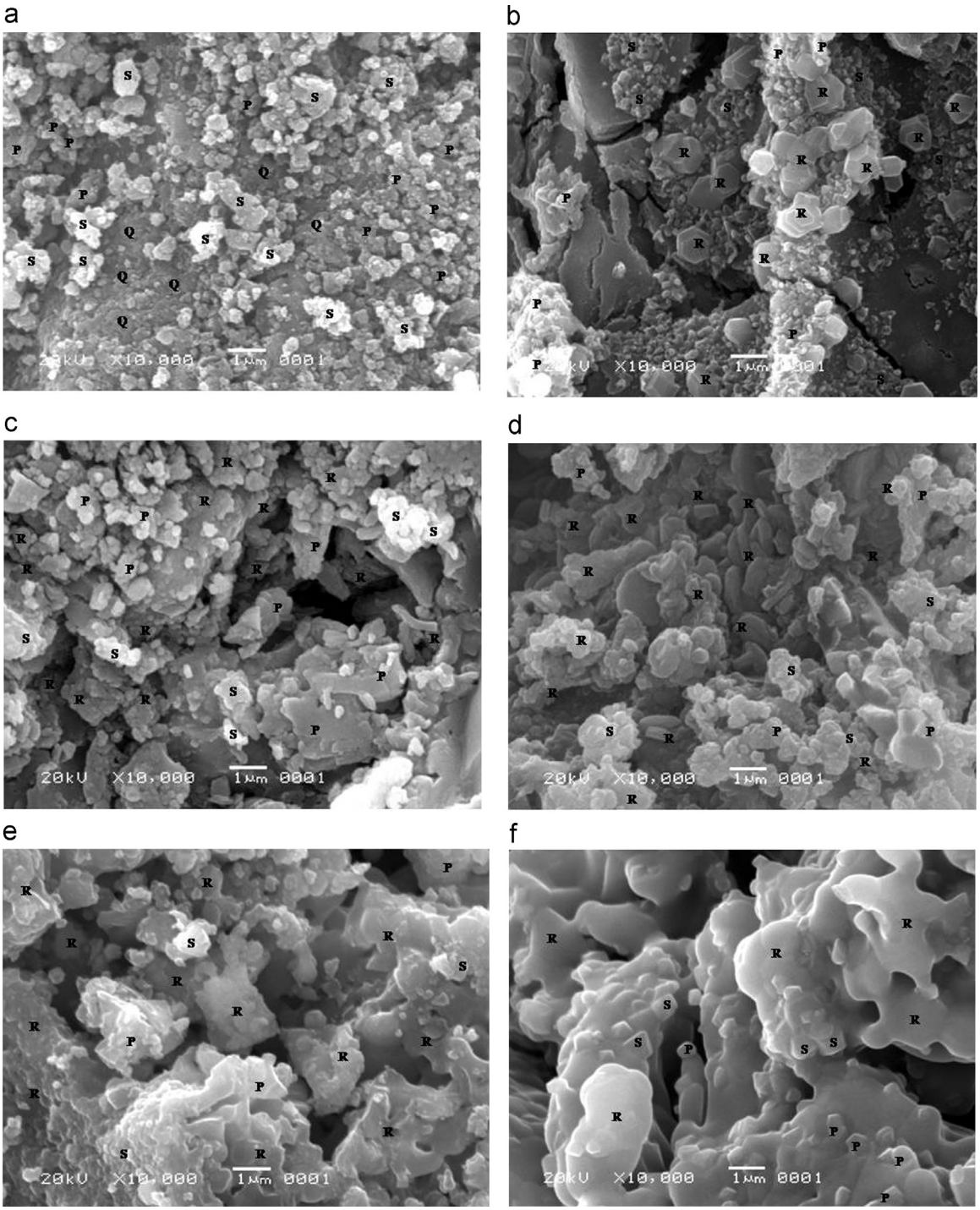

Fig. 4. The scanning electron microscopy (SEM) images of the samples sintered at different temperatures (a) 1050 °C, (b) 1110 °C, (c) 1170 °C, (d) 1230 °C, (e) 1290 °C, (f) 1350 °C. Accelerating voltage 20 kV, working distance 11 mm. P: spinel, Q: μ-cordierite, R: α-cordierite, S: cristobalite.

2.20 g/cm^3 as the sintering temperature increased from 1050 to 1230 °C. The density was slightly increased and reached the value of 2.30 g/cm^3 at the sintering temperature of 1350 °C. The slow decrease of the density with increasing temperature up to 1170 °C was attributed to the increased amount of spinel and cristobalite phases, followed by sharp decrease with increasing temperature up to 1230 °C. The change in density was most likely due to conversion of spinel and cristobalite into cordierite at 1230 °C, as displayed by the XRD results presented in Table 2, in which the significant changes in the quantity of the three phases were calculated. These results are in accordance with the results of others [53,54], in which it was reported that the density of spinel and cristobalite phases is higher than that of cordierite. In those previous studies, the density of spinel and cristobalite are 3.58 g/cm^3 and 2.6 g/cm^3, respectively, while for cordierite, the value is 2.3 g/cm^3 were reported.

The sharp decrease of porosity with increasing temperature up to 1230 °C was attributed to increased formation of cordierite phase, leading to decreased porosity. Beyond this temperature, density and porosity are slowly increased, probably indicating the domination of cordierite, narrower particles distances and also smaller pore in the samples as a result of higher sintering

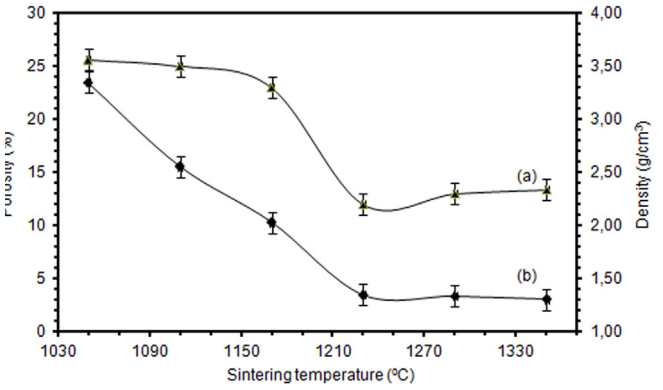

Fig. 5. Density (a) and Porosity (b) as a function of sintering temperatures.

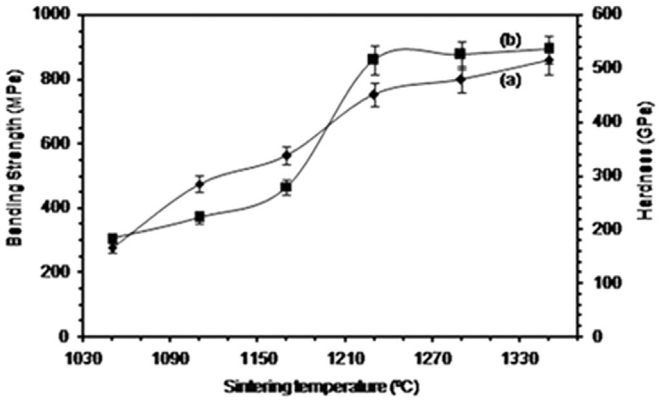

Fig. 6. Hardness (a) and Bending strength (b) as a function of sintering temperature.

temperature applied, which is in accordance with the surface morphologies of the samples as seen in SEM results (Fig. 4(d)–(e)). Moreover, the porosity was found to decrease as the sintering temperature increased (Fig. 5b), which is in agreement with the increase of the amount of cordierite (See Table 2). These findings implied that at temperature of 1230 °C, the sample has reached the vitrification point and transformed in glassy state, leading to suppression of porosity, as has been also suggested by others [55].

Fig. 6 shows the change in hardness and bending strength of the sintered samples, indicating that both characteristics increased as sintering temperature increased. As shown in Fig. 6a, the higher the sintering temperatures, the larger the hardness, which implies that the samples became more compact as a result of increased amount of cordierite (Table 2). The bending strength is sharply increased from sintering temperature of 1050 to 1230 °C and relatively stable up to 1230 °C, as indicated by the practically plat line. This profile suggests that the bending strength can be considered as fully associated with the cordierite phase. From practical point of view, this finding demonstrates that the hardness and bending strength of the samples can be controlled by controlling the formation of the cordierite phase, which is very useful for adjusting the suitability of the material for specified applications, such as insulator and conducting element in refractory devices. Other factors that control the hardness and bending strength are probably both the homogeneity of cordierite and the arrangement of the particles as a result of higher sintering temperatures applied, which is in accordance with the surface morphology of the samples, as shown in Fig. 4d–f.

Fig. 7 shows the change in thermal expansion coefficient of the samples as a function of sintering temperatures. The results reveal

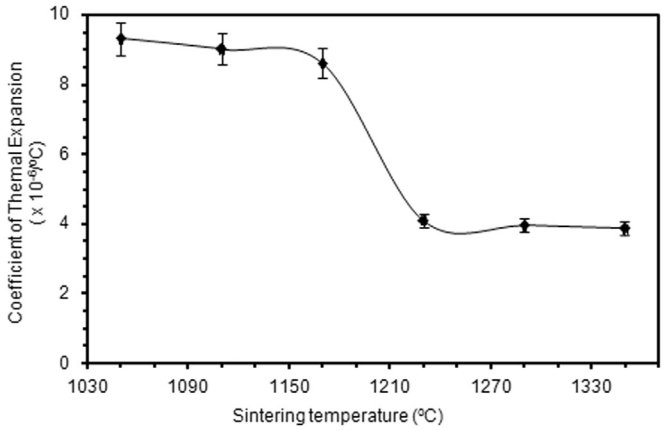

Fig. 7. Coefficient of thermal expansion of the sintered samples at different temperatures.

that the thermal expansion coefficient of the samples decreased slowly as the sintering temperatures increase from 1050 to 1170 °C and then dropped drastically from 8.5×10^{-6}/°C to 3.5×10^{-6}/°C when sintering temperatures increased from 1170 to 1230 °C, and then slightly decreased to the final value of 3.3×10^{-6}/°C at 1350 °C. It can be summarized that, as the sintering temperature increased, the coefficient of thermal expansion decreased, most probably due to the decrease in the amount of spinel and cristobalite, as supported by the previous study [17]. It is also found that the coefficient of thermal expansion decreased as the amount of cordierite increased and the porosity decreased. The trend observed in this study concerning thermal expansion coefficient is consistent with the relationship between thermal expansion coefficient and the volume fraction of the sample as described in the previous studies [56,57]. These previous studies explained that thermal expansion coefficient was proportional to the volume fraction of materials in the composite and inversed with the porosity. It can be seen that coefficient of thermal expansion of spinel is higher than those of cristobalite and cordierite, which are in agreement with the results described in previous study [54]. More specifically, it was reported that the coefficient of thermal expansion of spinel is 9×10^{-6}/°C and cristobalite is 2.6×10^{-6}/°C, and thermal expansion coefficient of cordierite is 2.65×10^{-6}/°C [19,58]. In accordance with the above values reported by others, it is then clear that decreased thermal expansion coefficient of the sample investigated in this study is most likely associated with the increased amount of cordierite, as a consequence of elevated sintering temperatures, as confirmed by XRD results (See Table 2).

4. Conclusions

This study demonstrated that refractory cordierite was successfully prepared using rice husk silica as raw materials. Sintering treatment from 1050 to 1350 °C revealed the formation of cordierite from the reaction between spinel and cristobalite phases. The formation of cordierite phase was evidently revealed by the XRD, in which at sintering temperatures of 1050 to 1170 °C the major phases are μ and α-cordierite, spinel and cristobalite, and when sintering temperatures were further increased to 1230–1350 °C, the cordierite emerged as a dominant phase, while spinel and cristobalite are practically undetected. Phase transformation was found to result in the change of the characteristics of the samples which related to cordierite formation, including decreased porosity, density, and thermal expansion coefficient. It also found that thermal treatments led to increased hardness as well as bending strength. Based on these characteristics, the samples are

considered as insulator, suggesting the potential use of the cordierite in refractory devices.

Acknowledgments

The authors wish to thank and appreciate the Directorate General of Higher Education Republic of Indonesia (DIKTI) for research funding provided through the Competency Research Grant Batch I Program 2015, with Contract number: 050/SPH2/PL/Dit. Litabmas/II/2015.

References

[1] Y. Kobayashi, K. Sumi, E. Kato, Preparation of dense cordierite ceramics from magnesium compounds and kaolinite without additives, Ceram. Int. 26 (2000) 739–743.
[2] M.E. Milberg, H.D. Blair, Thermal expansion of cordierite, J. Am. Ceram. Soc. 60 (1997) 372–373.
[3] A. Yamuna, R. Jhonson, Y.R. Mayajan, M. Lalithambika, Kaolin-Based cordierite for pollution control, J. Eur. Ceram. Soc. 24 (2004) 65–73.
[4] S. Kurama, H. Kurama, The reaction kinetics of rice husk based cordierite ceramics, Ceram. Int. 34 (2008) 269–272.
[5] K. Zhu, Y.D. Yang, J. Wu, R. Zhang, Synthesis of cordierite with low thermal expansion coefficient, Adv. Mater. 105–106 (2010) 802–804.
[6] E.M.A. Hamzawy, A.F. Ali, Sol gel preparation of boron containing cordierite $Mg_2(Al_{x4}B_x)Si_5O_8$ and its crystallization, Mater. Charact. 57 (4–5) (2006) 414–418.
[7] F.A.C. Oliveira, J.C. Fernandez, Mechanical and thermal behavior of cordierite zirconia composites, Ceram. Int. 28 (2002) 79–91.
[8] M.A. Camerucci, G. Urretavizcaya, M.S. Castro, A.L. Cavalieri, Electrical properties and thermal expansion of cordierite and cordierite-mullite materials, J. Eur. Ceram. Soc. 21 (16) (2001) 2917–2923.
[9] E. Salje, Structural states of Mg-cordierite II: Landau theory, Phys. Chem. Miner. 14 (1987) 455–460.
[10] R. Goren, C. Ozgur, H. Gocmez, The preparation of cordierite from talc, fly ash, fused silica and alumina mixtures, Ceram. Int. 32 (2006) 53–56.
[11] P. Laokula, S. Maensirib, Synthesis, characterisation and sintering behavior of nanocrystalline cordierite ceramics, Adv. Sci. Technol. 45 (2006) 242–247.
[12] J.R. González-Velasco, M.A. Gutiérrez-Ortiz, R. Ferret, A. Aranzabal, J.A. Botas, Synthesis of cordierite monolithic honeycomb by solid state reaction of precursor oxides, Mater. Sci. 34 (1999) 1999–2002.
[13] D.L. Evans, G.R. Fischer, J.E. Geiger, F.W. Martin, Thermal expansions and chemical modifications of cordierite, J. Am. Ceram. Soc. 63 (1980) 629–634.
[14] C. Ghitulica, E. Andronescu, O. Nicola, A. Dicea, M. Birsan, Preparation and characterization of cordierite powders, J. Eur. Ceram. Soc. 27 (2–3) (2007) 711–713.
[15] P. Zhu, L.Y. Wang, D. Hong, M. Zhou, A Study of cordierite ceramics synthesis from serpentine tailing and kaolin tailing, J. Sci. Sinter. 44 (2012) 129–134.
[16] R. Bejjaaoui, A. Benhammou, L. Nibou, B. Tanouti, J.P. Bonnet, A. Yacoubi, A. Ammar, Synthesis and characterization of cordierite ceramic from Morroccan stevensite and andalusite, Appl. Clay Sci. 40 (2010) 336–340.
[17] S. Rattanavadi, L. Punsukumtana, N. Thavarungkul, N. Srisukhumbowornchai, Cordierite composites using new source of waste; sludge cake from aluminum scrap and dross recycling industry in Thailand, J. Aus. Ceram. Soc. 50 (2) (2014) 118–125.
[18] E.M.M. Ewais, Y.M.Z. Ahmed, A.M.M. Ameen, Preparation of porous ceramic using a silica secondary resource (silica fumes) for dust filtration purposes, J. Ceram. Process. Res. 10 (6) (2009) 721–728.
[19] Z. Acimovic, L. Pavlovic, L. Trumbulovic, L. Andric, and Stamatovic, Synthesis and characterisation of the cordierite ceramic from non standard raw materials, for application in foundry, Mater. Lett. 57 (2003) 2651–2656.
[20] A. Benhammou, Y. El Hafiane, A. Abourriche, Y. Abouliatim, L. Nibou, A. Yaacoubi, N. Tessier Doyen, A. Smith, B. Tanouti, Effect of oil shale addition and sintering cycle on the microstructure and mechanical properties of porous cordierite-ceramic, Ceram. Int. 40 (2014) 8937–8944.
[21] P.N. Kumta, R.E. Hackenberg, P. McMichael, W.C. Johnson, Solution sol–gel synthesis and phase evolution studies of cordierite xerogels, aerogels and thin films, Mater. Lett. 20 (5–6) (1994) 355–362.
[22] R. Petrovič, Dj Janackovič, S. Zec, S. Drmanič, L.K. Gvozdenovič, Crystallisation behavior of alkoxy-derived cordierite gels, J. Sol–gel. Sci. Technol. 28 (1) (2003) 111–118.
[23] I. Jankovič-Castvan, S. Lazarevič, B. Jordovič, R. Petrovič, D. Tanaskovič, Dj. Janackovič, Electrical properties of cordierite obtained by non-hydrolytic sol-gel method, J. Eur. Ceram. Soc. 27 (13–15) (2007) 3659–3661.
[24] N.M. El-Buaishi, I. Jankovič-Castvan, B. Jokič, Dj Veljovič, Dj Janackovič, R. Petrovič, Crystallization behavior and sintering of cordierite synthesized by an aqueous sol–gel route, Ceram. Int. 38 (3) (2012) 1835–1841.
[25] B.C. Lim, H.M. Jang, Homogeneous fabrication and densification of cordierite zirconia composite by a mixed colloidal processing route, J. Am. Ceram. Soc. 76 (1993) 1482–1490.
[26] F.A.C. Oliveira, J.C. Fernandes, J. Schmitt, L.G. Rosa, D. Dias, Fracture toughness of dense cordierite: sintering, effect, Mater. Sci. Forum 730–732 (2013) 445–449.
[27] H. Suzuki, H. Saito, T. Hayashi, Thermal and electrical properties of alkoxy-derived cordierite ceramics, J. Eur. Ceram. Soc. 9 (5) (1992) 365–371.
[28] S. Sembiring, Synthesis and characterisation of rice husk silica based borosilicate (B_2SiO_5) ceramic by sol gel routes, Indones. J. Chem. 11 (1) (2011) 85–89.
[29] W. Simanjuntak, S. Sembiring, The use of the rietveld method to study the phase composition of cordierite ($Mg_2Al_4Si_5O_{18}$) ceramics prepared from rice husk silica, Makara J. Sci. 15 (1) (2011) 97–100.
[30] W. Simanjuntak, S. Sembiring, K. Sebayang, Effect of pyrolysis temperature on composition and electrical conductivity of carbosil prepared from rice husk, Indones. J. Chem. 12 (1) (2012) 119–125.
[31] W. Simanjuntak, S. Sembiring, P. Manurung, R. Situmeang, I.M. Low, Characteristics of aluminosilicates prepared from rice husk silica and aluminum metal, Ceram. Int. 39 (8) (2013) 9369–9375.
[32] S. Sembiring, W. Simanjuntak, X-ray diffraction phase analyses of mullite derived from rice husk silica, Makara J. Sci. 16 (2) (2012) 77–82.
[33] S. Sembiring, W. Simanjuntak, P. Manurung, D. Asmi, I.M. Low, Synthesis and characterisation of gel-derived mullite precursors from rice husk silica, Ceram. Int. 40 (5) (2014) 7067–7072.
[34] A.A.M. Daifullah, N.S. Awwad, S.A. El-Reefy, Purification of phosphoric acid from ferricion using modified rice husk, J. Chem. Eng. Proc. 43 (2004) 193–201.
[35] V.P. Della, I. Kuhn, D. Hotza, Rice husk ash an alternate source for active silica production, Mater. Lett. 57 (2002) 818–821.
[36] K. Amutha, R. Ravibaskar, G. Sivakumar, Extraction, synthesis and characterisation of nanosilica from rice husk ash, Int. Nanotechnol. Appl. 4 (1) (2010) 61–66.
[37] M. Subarna, P. Banerjee, S. Purakayasha, B. Ghosh, Silicon-doped carbon semiconductor from rice husk char, Mater. Chem. Phys. 109 (2008) 169–173.
[38] S.K. Singh, B.C. Mohanty, S. Basu, Synthesis of SiC from rice husk in a plasma reactor, Bull. Mater. Sci. 25 (6) (2002) 561–563.
[39] B. Karmakar, P. Kundu, S. Jana, R.N. Dwiredi, Crystallization kinetics and mechanism of low expansion lithium-alumino-silicate glass ceramics by dilatometry, J. Am. Ceram. Soc. 85 (10) (2002) 2572–2574.
[40] M. Chatterjee, M.K. Naskar, Sol-gel synthesis of lithium aluminum silicate powders; the effect of silica sources, Ceram. Int. 32 (2006) 623–632.
[41] JADE Program XRD Pattern Processing PC, Material Data Inc (MDI), Livermore, CA, 1997.
[42] B.A. Hunter, Software Rietica for 95/98 Window NT, Version 1, 1997, 70.
[43] R.T. Downs, M. Hall-Wallase, American Mineralogist Crystal Structure Database, 1997.
[44] Australian Standard, Refractories and refractory material physical test methods: The determination of density, porosity and water adsorption, 1–4, 1989, 1774.
[45] N. Nagai, H. Hashimoto, FTIR-ATR study of depth profile of SiO_2 ultra-thin films, Appl. Surf. Sci. 172 (3–4) (2001) 307–311.
[46] M. Sales, J. Alarson, Crystallization of sol–gel derived glass ceramic powders in the CaO MgO–Al_2O_3–SiO_2 system. Part II: cordierite, Mater. Sci. 30 (1995) 2341–2347.
[47] Dj Janackovič, V. Jokanovič, L.K. Gvozdenovič, S. Zec, Dj Uskokovič, Synthesis and formation mechanism of submicrometre spherical cordierite powder by ultrasonic spray pyrolysis, J. Mater. Sci. 32 (1997) 163–168.
[48] Powder Diffraction File (Type PDF-2). Diffraction Data for XRD Identification. International Centre for Diffraction data, PA, USA, 1997.
[49] M. Okiyama, T. Fukui, C. Sakurai, Effects of complex precursors on alkoxyde-derived cordierite powder, J. Am. Ceram. Soc. 75 (1) (1992) 153–160.
[50] M.K. Naskar, M. Chatterjee, A novel process for the synthesis of cordierite ($Mg_2M_4Si_5O_{18}$) powder from rice husk ash and other sources of silica and their comparative study, J. Eur. Ceram. Soc. 24 (13) (2004) 3499–3508.
[51] E.H. Kisi, Rietveld analysis of powder diffraction patterns, Mat. Forum 18 (1994) 135 153.
[52] E. Wu, E.H. Kisi, A.E.M. Gray, Modelling dislocation-induced anisotropic line broadening in Rietveld refinements using a voigt function II: application to voigt function neutron powder diffraction data, J. Appl. Cryst. 31 (1998) 363.
[53] I. Ganesh, Fabrication of magnesium aluminate ($MgAl_2O_4$) spinel foam, Ceram. Int. 37 (2011) 2237–2245.
[54] A.H. Charles, Handbook of Ceramic Glasses and Diamonds, Mc Graw Hills, Company Inc, USA, 2001.
[55] Frank, J. Hamer, The Potter's Dictionary of Materials and Technique, 5th ed., University of Pennsylvania, Philadelphia (2004), pp. 247–248.
[56] T. Ono, K. Matsumaru, I. Juarez-Ramirez, M. Leticia Torres-Martinez, K. Ishizaki, Development of porous material with high Young's Modulus and low thermal expansion coefficient in SiC-Vitrified bonding material-$LiAlSiO_4$ system, Mater. Sci. Forum 620–622 (2009) 715–718.
[57] P. Beatrice, K. Miroslav, K. Miriam K., Moisture expansion of porous biscuit bodies-reason of glaze cracking, Ceram. Silik. 46 (2002) 159–165.
[58] F. Aumento, Stability, Lattice parameters and thermal expansion of β-cristobalite, Am. Mineral. (1967) 543–544.